

ARTICLE

Fly Ash and Slag as Partial Replacement of Cement for the Synthesis of Low Carbon Cementitious Materials

Yafei Hu^{1,2}, Keqing Li^{1,2}, Lujing Zheng³ and Bin Han^{1,2,*}

¹School of Civil and Resource Engineering, University of Science and Technology Beijing, Beijing, 100083, China

²Key Laboratory of Ministry of Education of China for Efficient Mining and Safety of Metal Mines, University of Science and Technology Beijing, Beijing, 100083, China

³Mining College, Guizhou University, Guiyang, 550025, China

*Corresponding Author: Bin Han. Email: bin.han@ustb.edu.cn

Received: 23 June 2022 Accepted: 29 August 2022

ABSTRACT

Tailings known as solid waste are generated by the mining industry. The development of tailings as wet shotcrete aggregates has significant economic and environmental benefits. The fine particle size of the tailings results in a large consumption of traditional cement as a cementitious material and insignificant improvement in strength. Therefore, a composite cementitious system of cement and solid waste resources (fly ash and slag powder) is explored for this study. In this paper, the response surface methodology (RSM) is used to optimize the experimental design and a multivariate nonlinear response model with cement, fly ash and slag powder contents as variables are constructed, which can investigate the effect of the composite cementitious system on the strength of tailing wet shotcrete (TWSC). In addition, the information entropy (IE) is introduced and combined with the RSM to evaluate the composite cementitious system. Finally, the desirability function (DF) combined with RSM is used to optimize the composite cementitious system. The results show that the response model constructed in this paper has $R^2 = 0.96$ and P -value < 0.01 (the test result of the model is P -value < 0.01), which indicates that the model has high reliability. The higher the content of slag powder and cement in the composite cementitious system, the higher the strength and comprehensive score of the TWSC. There is a critical value of fly ash content, which makes the maximum cementation of the composite cementing system. The optimal mix proportion of the composite cementitious system is obtained based on RSM-DF, which leads to the strength of TWSC at different curing time to achieve the expected index.

KEYWORDS

Tailings; wet shotcrete; composite cementitious system; desirability function; mix proportion optimization

1 Introduction

Tailing is a solid mineral waste formed after the dewatering of tailings slurry discharged from mineral processing plants, which is one of the bulk solid wastes with the largest output and the lowest comprehensive utilization rate in China at present [1–3]. To improve the utilization rate of tailings, this paper proposes the concept of using tailings as aggregate instead of sand and gravel in wet shotcrete. Due to the extremely fine particles of tailings, it is difficult to achieve the strength requirements when using traditional cement as the



cementitious material, and if the cement dosage is increased, it must lead to high material cost [4,5]. In addition, the traditional cement production process consumes much energy and releases a lot of carbon dioxide, which is inconsistent with the current theme of green, low-carbon and environmental protection [6–8].

Supplementary cementitious materials (SCM), also known as volcanic ash, are typically derived from large, sustainable industrial and agricultural wastes and have potentially activatable hydraulic reactivity, which is used in the development of green cementitious materials at present [9–11]. Fly ash and slag are excellent SCMs. Fly ash is an industrial waste residue discharged from the pulverizing boilers of thermal power plants, which is an artificial volcanic ash material [12–14]. In the past, fly ash was commonly released into the atmosphere, but standards for air pollution control now require that it be captured by installing pollution control equipment prior to release [15–17]. Fly ash is commonly used as volcanic ash to produce hydraulic cement or hydraulic mortar, which can partially replace cement in concrete [18,19]. Granulated blast furnace slag is an industrial solid slag obtained by water quenching and granulation of molten material with calcium silicate as the main component when smelting pig iron in the blast furnace, which is mostly glassy and potentially water-hard cementitious activity [20,21]. Slag powder is a kind of high-quality admixture used to prepare concrete, which is a powder that conforms to the standard granulated blast furnace slag after being dried and ground to a considerable fineness and meeting the activity index [22,23]. Considering the excellent hydration and environmental characteristics of fly ash and slag powder, they are considered to replace part of cement to synthesize low-carbon cementitious materials.

Currently, relevant scholars have carried out research on the application of solid waste admixtures in concrete. Wen et al. developed a cementitious material using solid waste resources such as slag and fly ash, which enabled the cement paste backfill of coarse aggregate and fine tailings to achieve the strength requirements of mines while reducing the cost of filling [24,25]. Some scholars carried out a study on the effect of fly ash on the strength of concrete, which found that fly ash has the greatest effect on the compressive strength of concrete when the replacement rate of cement is within 30%, and the high dosage of fly ash leads to a reduction in strength [26,27]. Some other researchers studied the effect of slag powder on the strength and microstructure of silicate cement, which found that the incorporation of slag powder generated a large number of C-S-H gels and made the cement structure more compact and significantly increased the cement strength [28,29]. In addition, it was found that the right dosage of silica ash can shorten the setting time of cement and increase the compressive strength of shotcrete, which can promote the cement hydration reaction [30,31]. The above studies have shown that the incorporation of solid wastes such as slag powder into the cementitious material can significantly improve the mechanical properties of concrete and the doping material has the ability to partially replace cement. Therefore, solid wastes can be introduced into tailings wet shotcrete to improve its strength properties.

This paper optimizes the experimental design based on the response surface method to construct the strength response model of tailings wet shotcrete (TWSC) at different curing time, which can study the effects of cement, fly ash and slag powder dosage and their coupling effects on the strength of TWSC in the composite cementitious system. At the same time, the microstructure analysis of the TWSC is carried out with the aid of a scanning electron microscope to understand its microscopic morphology.

2 Materials and Methods

2.1 Materials

2.1.1 Tailings

The tailings from a gold mine in Guizhou Province, China, are used as the aggregate for the experiments. Its main chemical composition obtained by using X-ray fluorescence spectrometry (XRF) is shown in Table 1. Its activity index $M_a = 0.037$, which is basically inactive. This indicates that the tailing is suitable

for use as aggregates. The tailing with median particle size $D_{50} = 25 \mu\text{m}$ and particle size less than $75 \mu\text{m}$ account for about 90%. This indicates that the tailing is ultra-fine tailing. The particle size distribution of the tailing and X-ray diffraction (XRD) analysis are shown in Fig. 1.

Table 1: Chemical compositions of tailings (mass fraction) (%)

Materials	SiO ₂	CaO	MgO	Fe ₂ O ₃	Al ₂ O ₃	MnO	SO ₃	TiO ₂
Content	67.1	2.51	0.65	2.17	16.73	0.15	0.9	0.25

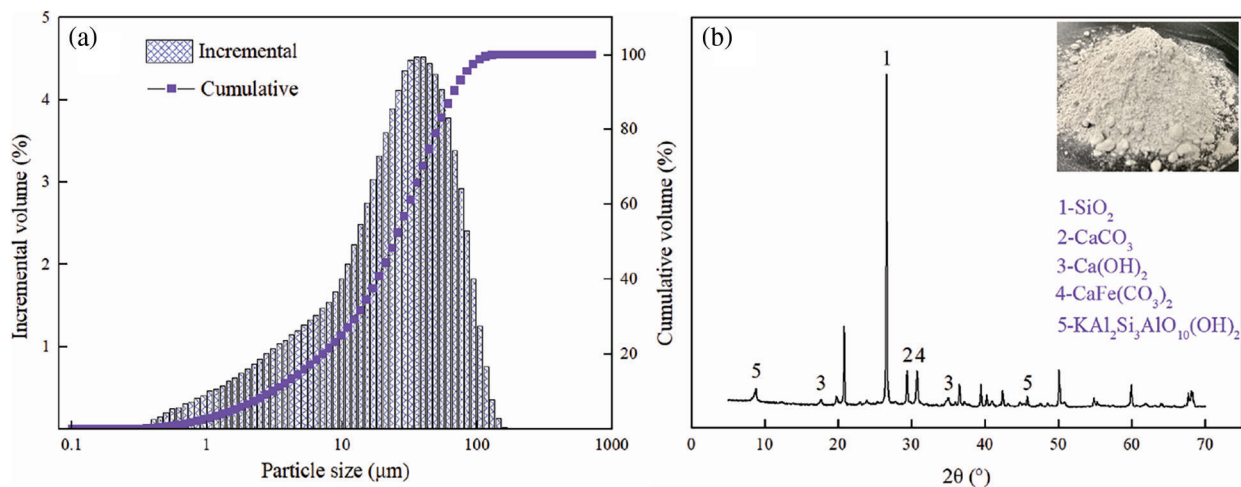


Figure 1: Particle size distribution and XRD analysis of tailings. (a) particle size distribution; (b) XRD analysis

2.1.2 Cementitious Materials

This paper uses cement, fly ash and slag powder to make a composite cementitious material. Cement is the activator, and fly ash and slag powder are the active materials. The physical and chemical characteristics of each material are as follows.

1. Cement type is PO42.5 silicate cement. Its density is 3.03 g/cm^3 , and the specific surface area is $380 \text{ m}^2/\text{kg}$. The initial setting time and final setting time are 150 min and 220 min, respectively. The 28 d compressive strength and flexural strengths are 54.3 and 8.7 MPa, respectively.
2. Fly ash is the main solid particulate waste emitted from coal-fired power plants. Its density is 2.55 g/cm^3 , and the specific surface area is $0.35 \text{ m}^2/\text{kg}$. From XRD analysis, it is clear that fly ash mainly contains mineral phases such as mullite, quartz and alumina. In addition, there are widening humps in the diffraction angle in the range of 10° – 30° . This indicates the presence of an amorphous phase and that the amorphous phase is a silica-alumina oxide vitreous.
3. Slag powder is granulated blast furnace slag. Its density is 2.9 g/cm^3 , and the specific surface area is $440 \text{ m}^2/\text{kg}$. The alkalinity, quality and activity coefficients are $M_0 = 1.17 (> 1)$, $K = 2.27 (> 1.8)$ and $M_a = 1.57$, respectively. This indicates that it is a highly reactive alkaline slag. From the XRD pattern, it can be seen that the slag powder contains a lot of active materials in glass phase crystals. This indicates that under normal conditions, the hydration reaction of slag powder is difficult and needs to be activated in order to have some hydration activity.

The chemical composition of the above materials obtained by using XRF is shown in Table 2, and the particle size distribution and X-ray diffraction (XRD) analysis are shown in Fig. 2.

Table 2: Chemical compositions of cementitious materials (mass fraction) (%)

Materials	SiO ₂	CaO	MgO	Fe ₂ O ₃	Al ₂ O ₃	SO ₃
Cement	20.35	62.20	4.22	3.17	4.34	2.54
Fly ash	45.1	5.6	1.13	0.85	24.2	2.1
Slag powder	27.51	43.24	8.09	0.38	16.25	1.51

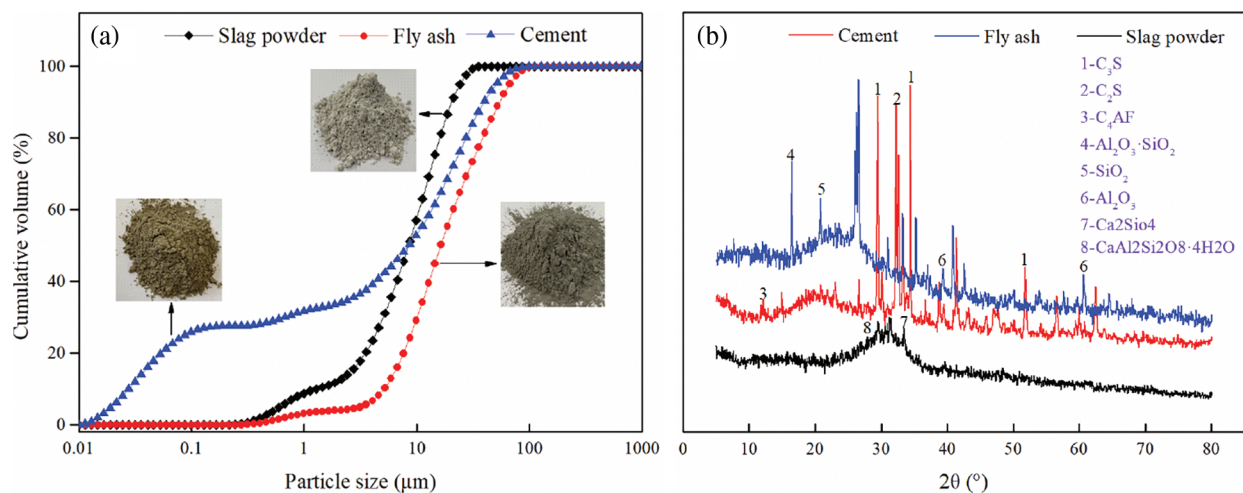


Figure 2: The particle size distribution and XRD analysis of cementitious materials. (a) particle size distribution; (b) XRD

2.2 Preparation of Cementitious Materials

Uniaxial compressive strength (UCS) is the important mechanical parameter of TWSC. For comparison, the three important variables in the 17 groups of experiments in this research, i.e., cement content, fly ash content, and slag powder content, are listed in Table 4. The materials were weighed according to the proportion of each group of experiments, then the materials were poured into a bucket and mixed for five minutes using a hand-held electric mixer. The mixed slurry was poured into a triplex test mold of size 15 cm × 15 cm × 15 cm and then vibrated for 2 min on a vibrating table of model ZS-15 to improve the compactness of the materials. The prepared specimens were put into the standard curing box for curing. The curing temperature is set to 20°C, and the curing humidity is set to 95%. After waiting for the specimens to be cured for 7, 14, and 28 days, the automatic pressure testing machine was used for UCS tests.

2.3 Experiment Design

In order to obtain the law and degree of effect of the composite cementitious system on the UCS of TWSC and to improve the experimental efficiency, RSM is used to optimize the experiment design. This is also used to analyze the effect of each variable on the UCS of TWSC and the comprehensive score of composite cementitious systems at different curing time. According to a large number of exploratory experiments, it is known that UCS and the flowability of concrete slurry can meet the construction requirements when the cement dosing, fly ash dosing and slag powder dosing are 440–520 kg/m³, 50–150 kg/m³ and 40–120 kg/m³, respectively.

The experiment is conducted with the content of cement, fly ash and slag powder as independent variables, denoted by X_1 , X_2 and X_3 , respectively. The 7, 14, and 28 d UCS of the tailing-based TWSC are the response quantity, denoted by Y_1 , Y_2 and Y_3 , respectively. The values of the variables taken in the experiment are: cement content of 440, 480 and 520 kg/m³, fly ash content of 50, 100 and 150 kg/m³, and slag powder content of 40, 80 and 120 kg/m³. The factors and levels of the RSM experiment design are shown in Table 3.

Table 3: RSM-BBD experimental factors and levels

Factors	Level code		
	-1	0	1
Cement content (X_1)	440	480	520
Fly ash content (X_2)	50	100	150
Slag powder content (X_3)	40	80	120

Table 4: Experimental results of RSM

Group	Factor			Measured values/MPa			Predicted values/MPa			Comprehensive score	
	X_1	X_2	X_3	Y_1	Y_2	Y_3	Y^*_1	Y^*_2	Y^*_3	M	M*
1	480	150	120	22.61	23.89	24.92	22.49	23.77	24.76	96.6	96.1
2	440	150	80	21.17	23.10	24.12	20.99	22.79	23.67	92.2	91.0
3	480	100	80	19.03	22.33	23.94	19.24	22.05	23.47	87.1	86.7
4	440	100	40	18.44	20.26	21.41	18.03	19.98	21.32	80.9	79.7
5	480	50	120	21.67	22.93	24.22	21.08	22.34	23.68	93.0	90.6
6	440	50	80	17.63	19.50	21.67	17.91	19.66	21.61	78.8	79.4
7	480	100	80	19.30	22.03	23.46	19.24	22.05	23.47	86.8	86.7
8	520	100	40	20.23	21.41	22.94	19.93	20.98	22.34	87.2	85.5
9	440	100	120	20.19	21.47	22.43	20.49	21.90	23.03	86.6	88.3
10	520	50	80	21.94	23.01	24.73	22.12	23.32	25.17	94.1	95.3
11	480	100	80	19.45	22.08	23.37	19.24	22.05	23.47	87.0	86.7
12	480	50	40	18.12	19.38	20.65	18.24	19.50	20.80	78.4	78.9
13	520	100	120	23.01	24.51	26.69	23.41	24.79	26.78	100.0	100.0
14	520	150	80	21.89	23.18	24.81	21.60	23.02	24.87	94.3	93.7
15	480	100	80	19.32	21.91	23.28	19.24	22.05	23.47	86.5	86.7
16	480	150	40	18.80	20.28	20.95	19.39	20.88	21.49	81.1	83.5
17	480	100	80	19.09	21.92	23.33	19.24	22.05	23.47	86.1	86.7

2.4 UCS Test

UCS is a key factor in evaluating the mechanical properties of TWSC and is the main indicator examined by mines to develop standards for TWSC [32,33]. When the TWSC specimens reach the corresponding

curing time, the automatic press is used to perform UCS testing on the specimens. Three TWSC specimens are made for each curing time, and the final UCS is taken as the average of the three specimens.

2.5 SEM Analysis

The scanning electron microscopy (SEM) method has been widely used to analyze the microstructural of concrete and its components since the 1960s, and it is recommended as a standard by ASTM to study concrete and who are familiar [34,35]. The TWSC is a cement-based material used in mines, and its micro-properties are often tested by SEM. As shown in Fig. 3, a Quanta FEG 250 field-emission electron microscopy system with an accelerating voltage of 10 kV is used to test the specimens of TWSC without the UCS test, and the influence of the coupling factors on the microstructural properties of the TWSC is studied.

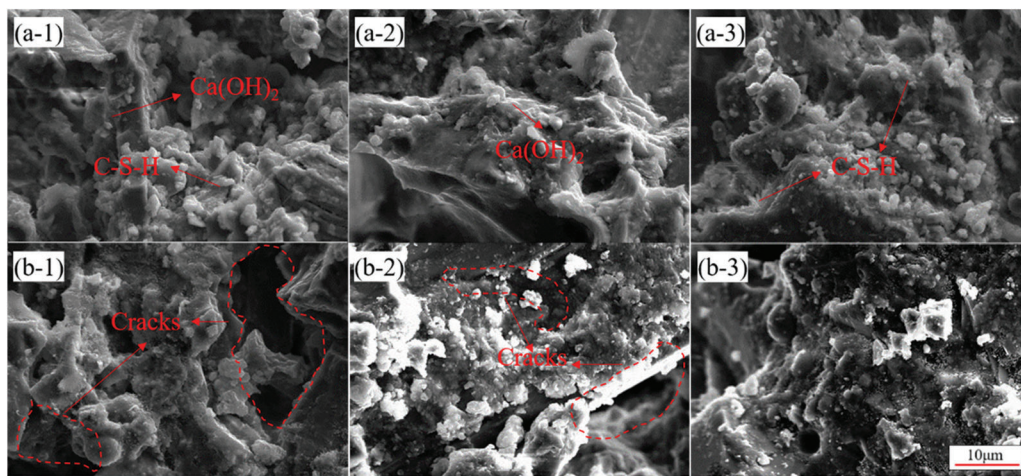


Figure 3: The results of SEM analysis for representative groups. (a) Results of group 13; (b) Results of group 16

2.6 Response Surface Methodology

Response Surface Methodology (RSM) is an experimental analysis method that combines a rational experimental design with a multiple regression equation [36–38]. This paper uses a multiple quadratic regression equation to fit the functional relationship between each effect factor and the response value. The principle is to search experimentally for the response surface function $y = f(x_1, x_2, \dots, x_m)$ between the effect factor x_i ($1 < i < m$) and the measured value y and make $y^* \rightarrow y$. Commonly used quadratic response surface function equations are as follows:

$$y^* = b_0 + \sum_{j=1}^m b_j x_j + \sum_{k < j < m} b_{kj} x_k x_j + \sum_{j=1}^m b_{jj} x_j^2 \quad (1)$$

In Eq. (1), y^* is the response value of the measured value; b_0 is a constant term; b_j , b_{kj} and b_{jj} are the regression coefficients of the primary, secondary and cross terms, respectively; m is the number of factors.

The experimental data are substituted into Eq. (1), and the least squares method is used to find the minimum value of the sum of squared errors. Finally, the response surface function corresponding to the independent variable can be found.

2.7 Information Entropy

Information Entropy (IE) is a mathematical abstraction that can be understood as the probability of occurrence of a certain kind of information [39]. When a message is more frequently appearing, it is more widely disseminated. In addition, IE can indicate the value of information from the perspective of information dissemination [40,41]. Therefore, IE value can be used as a measure of high or low information value. In this paper, IE is introduced to study the degree of influence of all effect factors on different response quantities and to score them together. This method is used to determine the level of effect of each factor on the responsiveness to avoid subjective elements and the one-sidedness of a single factor in the calculation.

Different factors X are used as indicators, and IE is used to calculate the weight coefficients and comprehensive scores M for each response quantity Y. This is used to determine the effect of each factor on different response quantities. The calculation steps are as follows:

1. Constructing the original index evaluation matrix $(Y_{ij})_{mn}$.
2. Constructing a probability matrix based on the original index evaluation matrix $(P_{ij})_{mn}$.

$$P_{ij} = X_{ij} / \left(\sum_{j=1}^n X_{ij} \right) \quad (2)$$

3. Calculating the IE of each evaluation index H_{ij} .

$$H_{ij} = - \sum_{j=1}^n (P_{ij} \times \ln P_{ij}) / \ln n \quad (3)$$

4. Calculating the weight coefficient of each index according to the IE of each index W_i .

$$W_i = (1 - H_i) / \sum_{i=1}^n (1 - H_i) \quad (4)$$

5. The equation for the comprehensive scoring index M is as follows:

$$M = \left(\frac{Y_1}{Y_{1\max}} \right) \times W_1 + \left(\frac{Y_2}{Y_{2\max}} \right) \times W_2 + \dots + \left(\frac{Y_i}{Y_{i\max}} \right) \times W_i \quad (5)$$

6. Constructing response surface functions for X and M using RSM.

$$M = d_0 + \sum_{j=1}^m d_j x_j + \sum_{k < j < m} d_{kj} x_k x_j + \sum_{j=1}^m d_{jj} x_j^2 \quad (6)$$

2.8 Desirability Function

The traditional RSM can only solve for single response quantities separately based on constraints, which is a major limitation. RSM cannot optimize multiple response values at the same time and thus cannot obtain the optimal solution that includes multiple factors to satisfy all response values. Therefore, Multi-objective Optimization based on Desirability Function (DF) combined with RSM is considered for multi-objective solving [42–45]. The following single DF is constructed according to different response models:

$$d_i(Y_i) = \begin{cases} 0 & (Y_i < T_i) \\ \frac{Y_i - T_i}{Z_i - T_i} & (T_i \leq Y_i \leq Z_i) \\ 1 & (Y_i > Z_i) \end{cases} \quad (7)$$

$$d_i(Y_i) = \begin{cases} 0 & (Y_i > Z_i) \\ \frac{Y_i - Z_i}{T_i - Z_i} & (T_i \leq Y_i \leq Z_i) \\ 1 & (Y_i < T_i) \end{cases} \quad (8)$$

$$d_i(Y_i) = \begin{cases} 0 & (Y_i \leq T_i) \\ \frac{Y_i - T_i}{N_i - T_i} & (T_i \leq Y_i < N_i) \\ 1 & (Y_i = N_i) \\ \frac{Z_i - Y_i}{Z_i - N_i} & (N_i \leq Y_i < Z_i) \\ 0 & (Y_i > Z_i) \end{cases} \quad (9)$$

In Eqs. (7)–(9), d_i is the DF of the i th response surface; Y_i is the i th response value; T_i , Z_i and N_i are the lower limits, upper limit and optimal target value of the i th response value, respectively. Eq. (7) is used to calculate the condition that the larger the response value and the higher the desirability; Eq. (8) is used to calculate the condition that the smaller the response value and the higher the desirability; Eq. (9) is used to calculate the condition that the larger the target value and the higher the desirability when it has the response target value. The weighted geometric mean multi-objective optimization function of each DF is constructed based on the calculation results. This is the comprehensive DF as follows:

$$D = \left(\prod_{i=1}^t d_i^{e_i} \right)^{\frac{1}{\sum e_i}} \quad (10)$$

In Eq. (10), t is the number of response values; e_i is the weight which depends on the importance of the different response values.

3 Discussion and Results

3.1 The Results of Compressive Strength

The experimental results of RSM are shown in Table 4.

3.2 Surface Morphology

The representative group 13 ($M = 100$) and group 16 ($M = 83.5$) of the RSM experimental results are selected for SEM analysis. The results are shown in Fig. 3. From Fig. 3a, it can be seen that the structure of specimens at different curing time is complete, and the hydration products are filled between the solid particles, thus forming a dense cementation structure, which is the main reason for the higher comprehensive score of this experimental group. This group has a relatively reasonable composite cementitious system with high cement and slag powder content and the addition of an appropriate amount of fly ash, which makes the strength structure of TWSC more complete. From Fig. 3b, it can be seen that there are a large number of pores and relatively few hydration products in the internal structure of this group of specimens at a curing time of 7 d. With the increase in the curing time, the internal structure of this group of specimens gradually tightened, but some porosity still existed. The internal structure still has defects leading to poor UCS performance. The above study shows that the composite cementitious system of this group has an unreasonable proportion (low cement and slag powder content and high fly ash content).

3.3 Modeling for UCS and Compressive Score

The regression model of UCS with the content of cement, fly ash, and slag powder can be constructed by substituting the experimental results of RSM into Eq. (1).

$$Y_1 = 19.24 + 1.21X_1 + 0.64X_2 + 1.49X_3 - 0.9X_1X_2 + 0.26X_1X_3 + 0.065X_2X_3 + 0.79X_1^2 + 0.63X_2^2 + 0.44X_3^2, R^2 = 0.964 \tag{11}$$

$$Y_2 = 22.05 + 0.97X_1 + 0.7X_2 + 1.43X_3 - 0.86X_1X_2 + 0.47X_1X_3 + 0.015X_2X_3 + 0.22X_1^2 - 0.075X_2^2 - 0.36X_3^2, R^2 = 0.952 \tag{12}$$

$$Y_3 = 23.48 + 1.19X_1 + 0.44X_2 + 1.54X_3 - 0.59X_1X_2 + 0.68X_1X_3 + 0.1X_2X_3 + 0.52X_1^2 - 0.16X_2^2 - 0.63X_3^2, R^2 = 0.949 \tag{13}$$

The experimental results of RSM are substituted into Eqs. (2)–(5), and the comprehensive scores of composite cementitious systems under each group of experimental conditions are calculated. The above results are shown in Table 3. Each comprehensive score is substituted into Eq. (6), and a regression model of the comprehensive score with the content of cement, fly ash and slag powder is constructed as follows:

$$M = 0.87 + 0.046X_1 + 0.025X_2 + 0.061X_3 - 0.033X_1X_2 + 0.018X_1X_3 + 0.002X_2X_3 + 0.023X_1^2 + 0.009X_2^2 - 0.003X_3^2, R^2 = 0.960 \tag{14}$$

The predictions of UCS and comprehensive scores are made based on the above model. The predicted values and predicted effect are shown in Table 4 and Fig. 4. From Fig. 4, the maximum error of the regression model is 3.1%, which indicates the high prediction accuracy of the model.

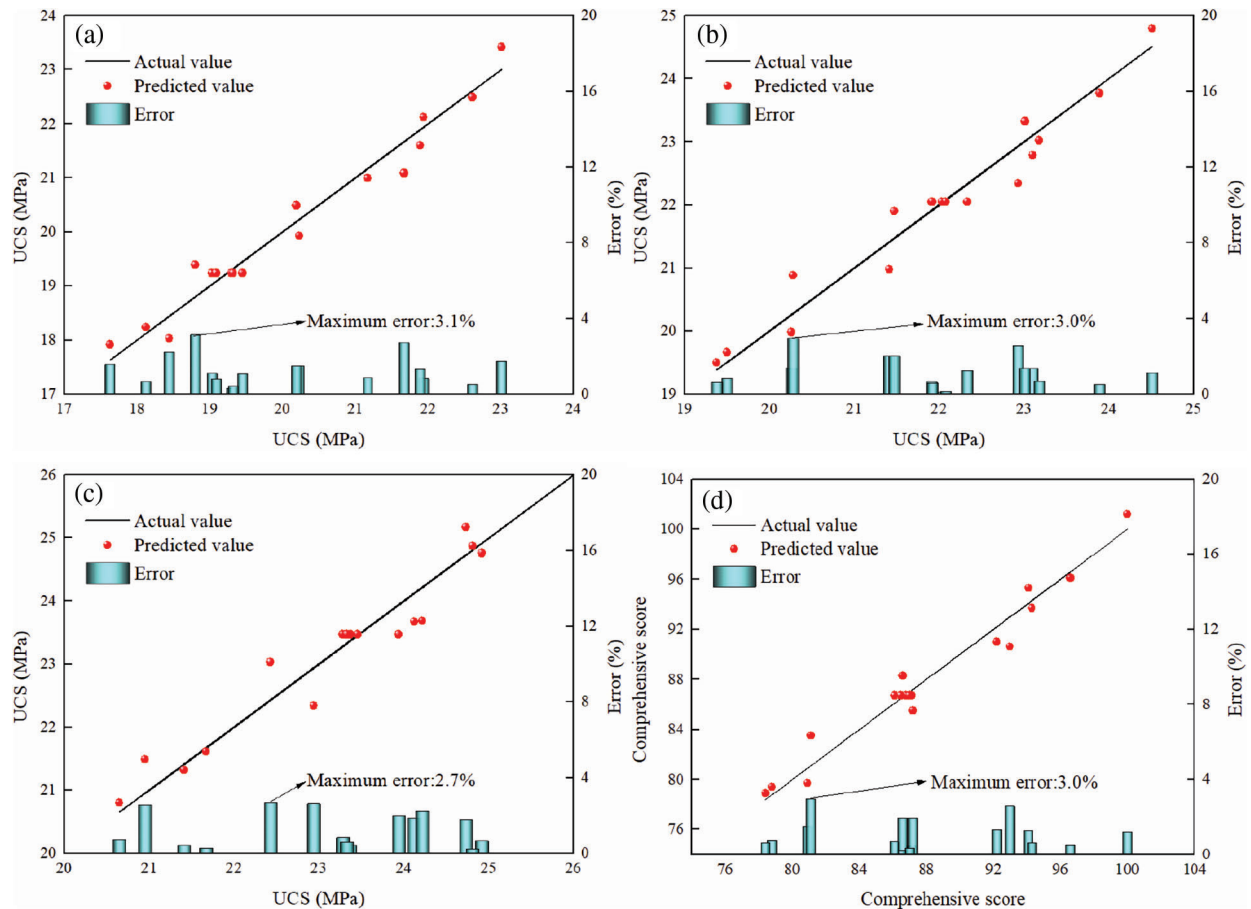


Figure 4: Effect of interaction between fly ash and slag powder on strength. (a) 7 d; (b) 14 d; (c) 28 d; (d) comprehensive score

3.4 Testing of the Model

In order to analyze the validity of the regression model, the variance analysis of the above regression equation is shown in Table 5. From Table 5, it can be seen that the model constructed in this paper has a P -value < 0.01 (highly significant), which indicates that the model has high reliability [46–48]. The correlation coefficient (R^2) tends to be close to 1, which indicates a well-fitting model. The F -value $> F_{0.95}(3, 17) = 3.2$, which indicates that the model is significant and statistically significant to reflect well the relationship between the variables of interest. Therefore, the regression model can be used to carry out the correlation analysis between the composite cementitious system and the UCS of the TWSC.

Table 5: Variance analysis of response surface experiment results

Source	F-value				P-value			
	Y ₁	Y ₂	Y ₃	M	Y ₁	Y ₂	Y ₃	M
Model	20.5	15.5	14.3	18.8	0.0003	0.0008	0.0010	0.0004

3.5 UCS Effect of TWSC

3.5.1 Single Factor Effect Analysis

The relationship between the single factor and UCS is shown in Fig. 5. From Fig. 5a, it can be seen that the UCS is gradually enhanced with the increase of cement content. The UCS is enhanced by 1.0%, 2.7% and 2.0% at 7 d, 14 d and 28 d, respectively, when the cement content is increased from 440 to 472 kg/m³. When the cement content is increased from 472 to 520 kg/m³, the 7 d, 14 d and 28 d UCS are enhanced by 11.6%, 6.3% and 8.3%, respectively. This indicates that the effect of cement on UCS enhancement is more significant when the cement content is more than 472 kg/m³. From Fig. 5b, it can be seen that with the increase of fly ash content, UCS first enhances and then weakens. This means that there is critical content to maximize the UCS and the critical content in this paper is 95 kg/m³. Overall, the effect of fly ash content on UCS is low. From Fig. 5c, it can be seen that UCS enhances with the increase of slag powder content. In addition, the magnitude of UCS enhancement gradually slows down when the slag powder content is more than 88 kg/m³. This indicates that there is a critical content that makes the UCS no longer enhance when the slag powder content continues to increase. From XRD analysis, it is clear that the slag powder contains a large number of active substances of glass phase crystals that need to be excited to have certain hydration activity. Therefore, when the activator is lacking, increasing the slag powder content cannot make the UCS continue to be enhanced.

3.5.2 Multi-Factor Coupling Effect on UCS

The effect of multi-factor coupling on the UCS of TWSC is shown in Figs. 6–8. From Fig. 6, under the coupling effect of cement and fly ash, TWSC has the highest strength under the condition of low fly ash content and high cement content. In addition, there is a critical value of cement content that shifts the effect of fly ash on the UCS of TWSC from enhancement to weakening at 7 d, 14 d and 28 d. Taking the 7 d UCS as an example, the UCS of TWSC enhances with the increase of fly ash content when the cement content is lower than 480 kg/m³. The UCS of TWSC weakens with the increase of fly ash content when the cement content is higher than 480 kg/m³. Moreover, the 7 d UCS of TWSC increases by 17.7% when the cement content is 440 kg/m³ and the fly ash content is increased from 50 to 150 kg/m³. However, when the cement content is 470 kg/m³, and the fly ash content is increased from 50 to 150 kg/m³, the 7 d UCS of TWSC is increased by only 5.6%. This indicates that the enhancement of UCS of TWSC by fly ash is more significant under the condition of low cement content. Overall, the UCS of TWSC is significantly enhanced with the increase of cement content when the fly ash content is

low. This indicates that the addition of appropriate amount of fly ash to the composite cementitious system can enhance the activity of cement and improve the UCS of TWSC.

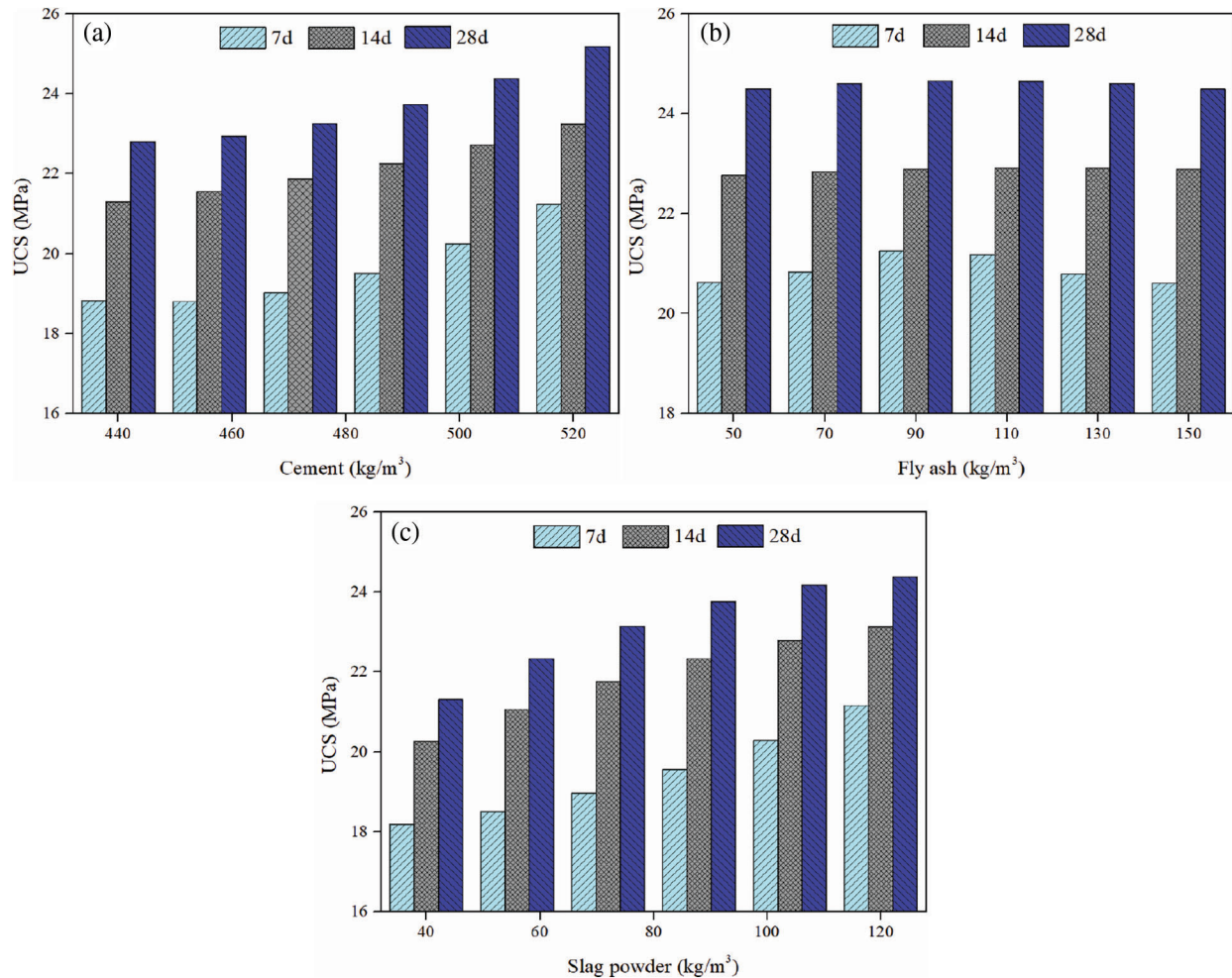


Figure 5: Effect of single factor on UCS. (a) cement content; (b) fly ash content; (c) slag powder content

As can be seen in Fig. 7, the 7 d, 14 d, and 28 d UCS exhibit the same characteristics under the coupling of cement and slag powder. The higher the content of cement and slag powder, the higher UCS. The 7 d, 14 d and 28 d UCS of TWSC increase by 30.8%, 21.5% and 26.5%, respectively, when the cement content is increased from 440 to 520 kg/m³ and the slag powder content is increased from 40 to 120 kg/m³. From XRD analysis, it is clear that slag powder has high potential activity. The Ca(OH)₂ generated by the hydration reaction activates the potential activity of the slag powder and generates more gel, which can enhance the UCS.

From Fig. 8, it can be seen that UCS is enhanced with the increase of fly ash and slag powder content. This indicates that the coupling of fly ash and slag powder has a positive effect on UCS. In addition, fly ash and slag powder have a mutual promotion effect. With the increase in the curing time, this promotion effect is more significant. In addition, there is a critical value of fly ash content that reduces the enhancement of TWSC by slag powder at 7 d, 14 d and 28 d UCS. When the fly ash content is lower than 90 kg/m³, the increase of slag powder content enhances the UCS of TWSC by 15.5%, 12.3% and 14.3% at 7 d, 14 d

and 28 d, respectively. When the fly ash content is higher than 90 kg/m^3 , the increase of slag powder content only enhances the 7 d, 14 d UCS and 28 d UCS of TWSC by 11.6%, 6.6% and 11.1%, respectively.

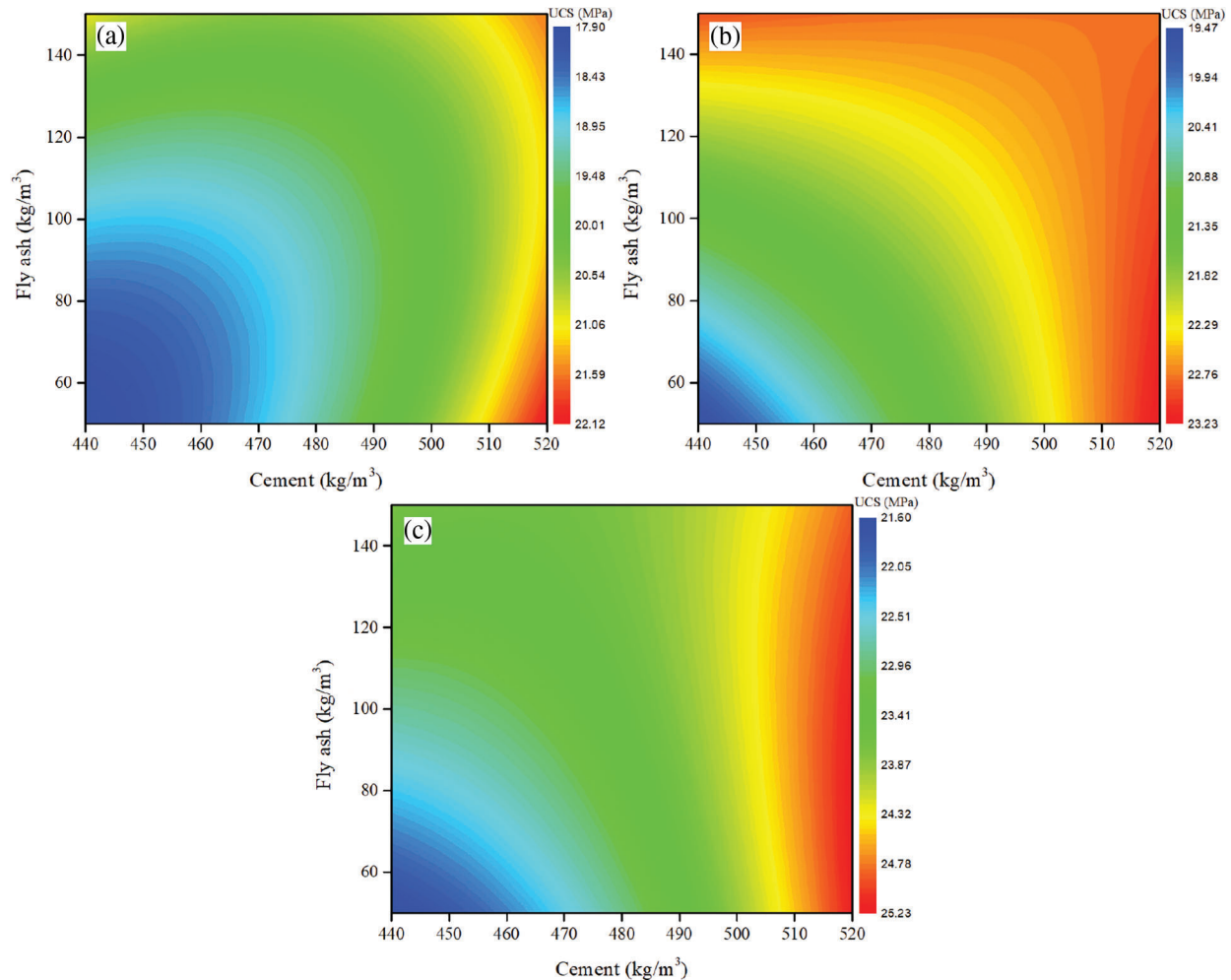


Figure 6: Results of UCS development for coupling effect of cement and fly ash. (a) 7 d; (b) 14 d; (c) 28 d

3.6 Effect of Composite Cementitious System on the Comprehensive Score

The comprehensive score reflects the influence of the composite cementitious system on the comprehensive UCS (containing 7 d, 14 d and 28 d UCS) of the TWSC, which is an evaluation of the reasonableness of the composite cementitious system.

3.6.1 Single Factor Effect Analysis on the Comprehensive Score

The effect of a single factor on the comprehensive score is shown in Fig. 9. As can be seen from Fig. 9, the comprehensive score increased as the level code (content) of each factor level increased. When the level code is less than 0, fly ash content has the greatest effect on the comprehensive score, followed by cement content, and slag powder content has the least. When the level code is greater than 0, the effect of fly ash content on the comprehensive score decreases and the effect of cement content and slag powder content on the comprehensive score becomes larger. This indicates that fly ash content should be controlled and increase cement and slag powder content in the composite cementitious system.

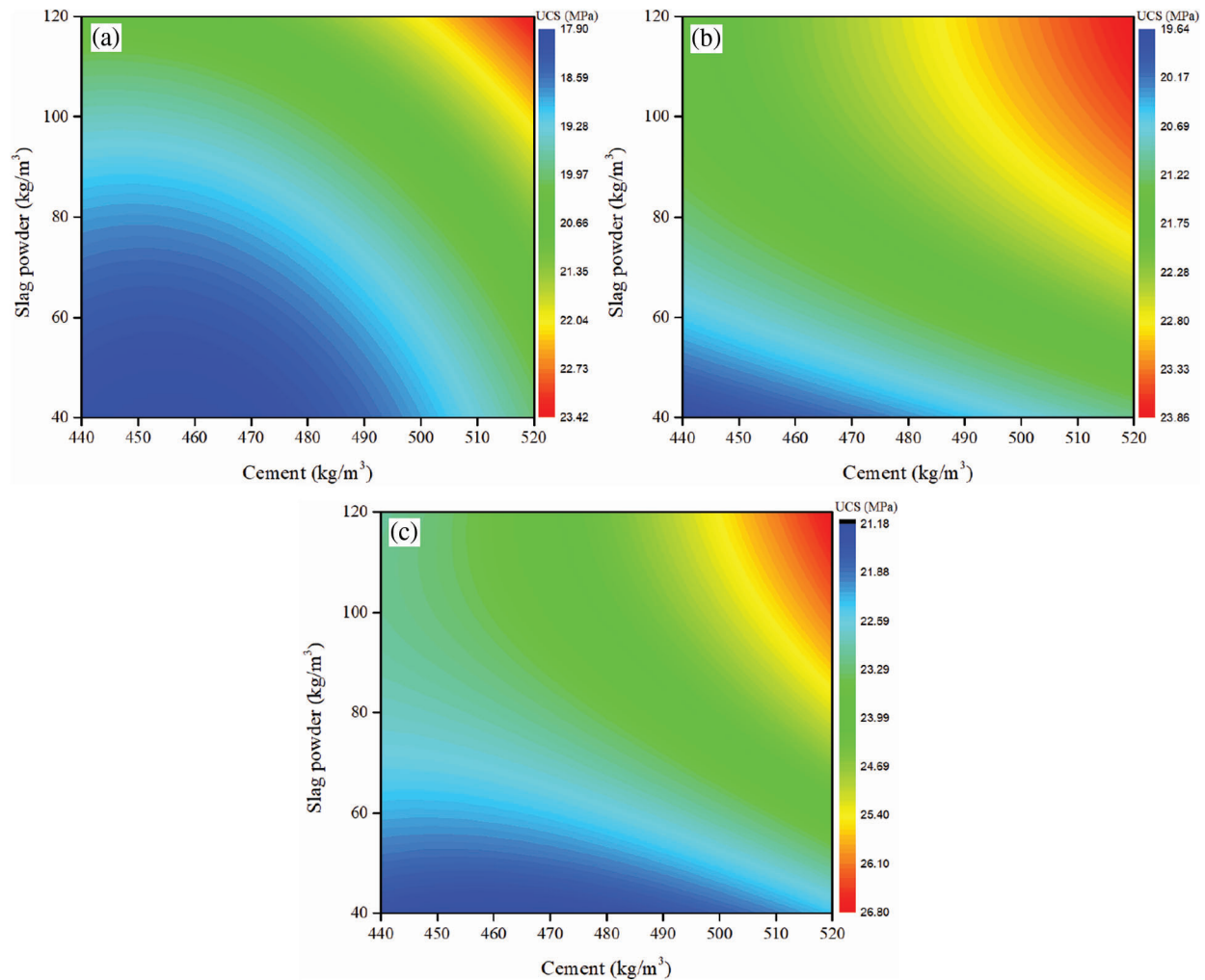


Figure 7: Results of UCS development for coupling effect of cement and slag powder. (a) 7 d; (b) 14 d; (c) 28 d

3.6.2 Multi-Factor Coupling Effect on the Comprehensive Score

The response surface of the comprehensive score under the coupling effect of multiple factors is shown in Fig. 10. From Fig. 10a, it can be seen that the comprehensive scores under the coupling effect of cement and fly ash all increase with the increase of cement content. This indicates that the cement positively affects the comprehensive score regardless of the change in fly ash content. However, at low cement content (<495 kg/m³), the comprehensive score increases with increasing fly ash content, and at high cement content (>495 kg/m³), the effect of fly ash content on the comprehensive score is not significant. From Fig. 10b, it can be seen that the comprehensive score under the coupling effect of cement and slag powder increases with the increase of both contents. The effect of slag powder on the comprehensive score at low cement content is not significant, and the comprehensive score at high cement content increases significantly with the increase of slag powder content. This indicates that cement and slag powder has the property of mutual activation, and this is consistent with the results of the above study. From Fig. 10c, it can be seen that the response surface under the coupling effect of slag powder and fly ash shows an increasing trend. This indicates that the coupling effect of the two factors has a positive effect on the comprehensive score. In addition, slag powder has a more significant improvement on the comprehensive score at low fly ash content than at high fly ash content.

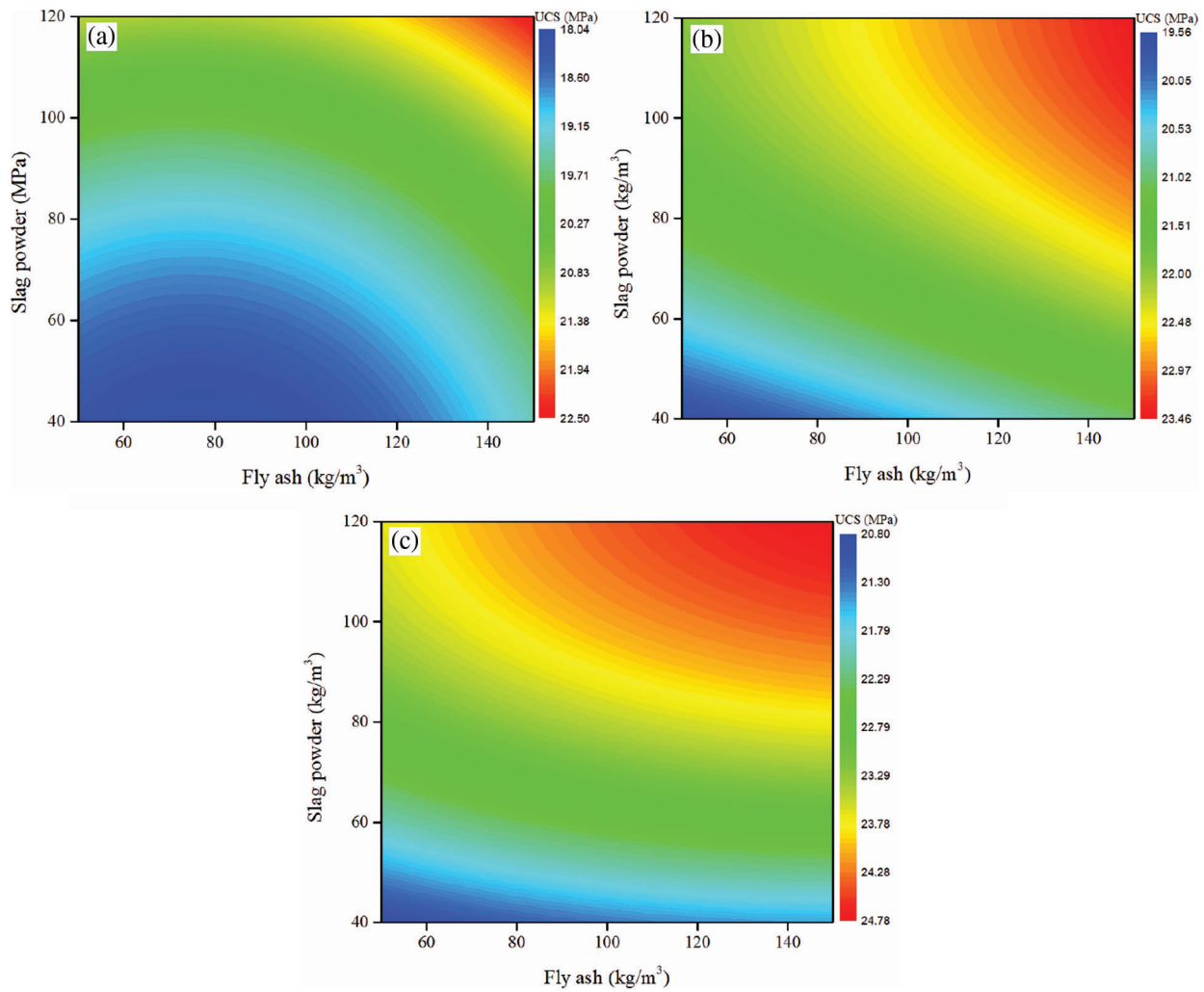


Figure 8: Results of UCS development for coupling effect of slag powder and fly ash. (a) 7 d; (b) 14 d; (c) 28 d

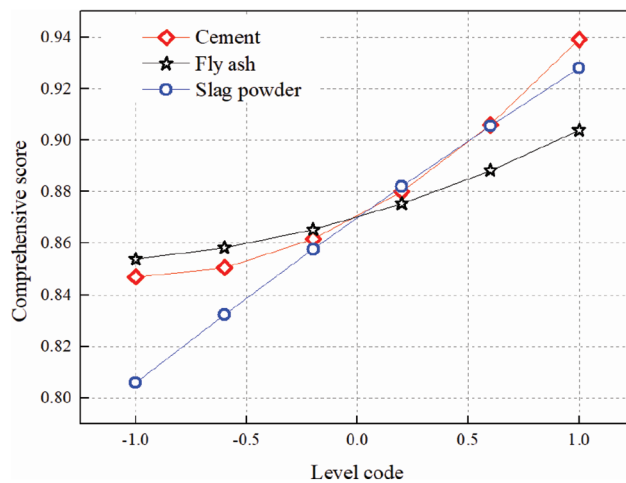


Figure 9: Effect of single factor on comprehensive score

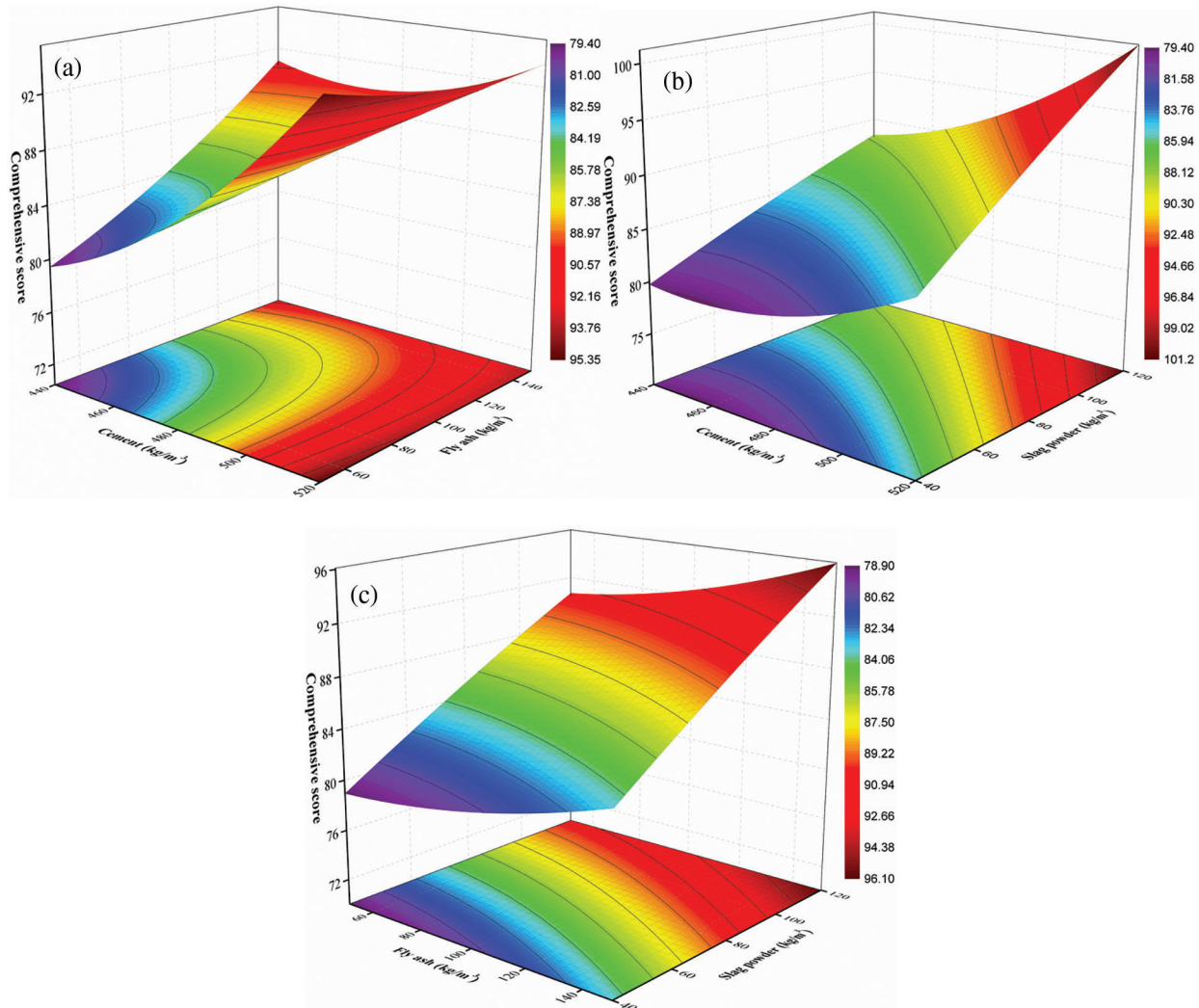


Figure 10: Effect of coupling factors on comprehensive score. (a) Cement and fly ash; (b) Cement and slag powder; (c) Fly ash and slag powder

3.7 Model Optimization

3.7.1 The Mix Proportion Optimization of TWSC

The rock mass of the mine studied in this paper is in a fractured state, and all the underground tunnels are supported by wet shotcrete (strength grade C20). In the population distribution of the ultimate compressive strength of cubes, the UCS with 95% guarantee measured by the standard experimental method is used as the concrete strength grade [49–51]. The above parameters are based on the concrete structure design code (GB50010-2010). To ensure that the UCS meets the standard, the strength guarantee rate is set to 85% in this paper. This means that 28 d UCS should be 23.5 MPa; 14 d UCS is 90% of 28 d (21.2 MPa); and 7 d UCS is 80% of 28 d (18.8 MPa). The experimental results based on RSM are used for multi-objective optimization using DF. The flow of RSM-DF multi-objective optimization is shown in Fig. 11.

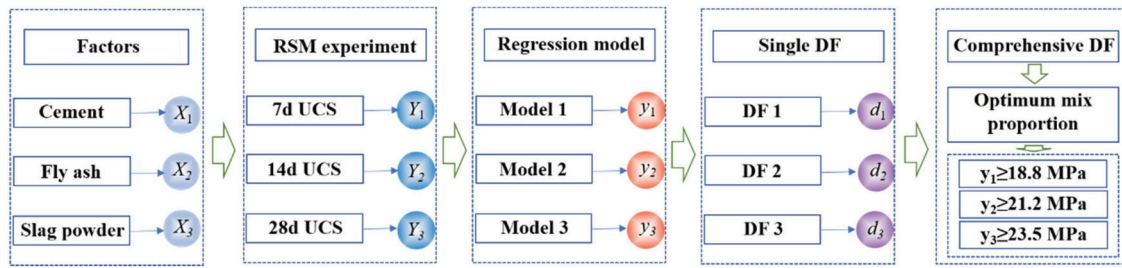


Figure 11: The flow of RSM-DF multi-objective optimization

The optimization range of 7 d UCS, 14 d UCS and 28 d UCS is set to 16.5–23.5 Mpa, 19–25 Mpa and 20.5–27 Mpa, respectively. The target values of optimization are set to 18.8, 21.2 and 23.5 Mpa. According to the support technique of this mine, it is known that the importance of UCS with different curing time is ranked as 28 d > 7 d > 14 d. Therefore, the weights of optimization targets are set as 0.5, 0.3 and 0.2 respectively. According to Eqs. (9) and (10), the single desirability and comprehensive desirability of UCS are calculated, and the influence law of different factors on the desirability is shown in Fig. 12. From Fig. 12a, it can be seen that the effect of slag powder content on single desirability is highly significant and the value of single desirability increases and then decreases with the increase of slag powder content. The single desirability is maximum when the slag powder content is in the range of 85–95 kg/m³. The effect of fly ash content on the single desirability is inferior, and the fluctuation of the single desirability within the experimental range is only 0.16. The cement content has a significant effect on the single desirability. When the cement content is around 480 kg/m³, the single desirability is maximum. Based on the above analysis, the comprehensive desirability under multiple factors is calculated by setting the cement content to 470–490 kg/m³ and the slag powder content to 85–95 kg/m³ and using fly ash content as the independent variable. The results are shown in Fig. 12b. From Fig. 12b, it can be seen that the comprehensive desirability of the composite cementitious system has a maximum value of 0.96 when the cement, fly ash, and slag powder content are 470, 80 and 90 kg/m³, respectively.

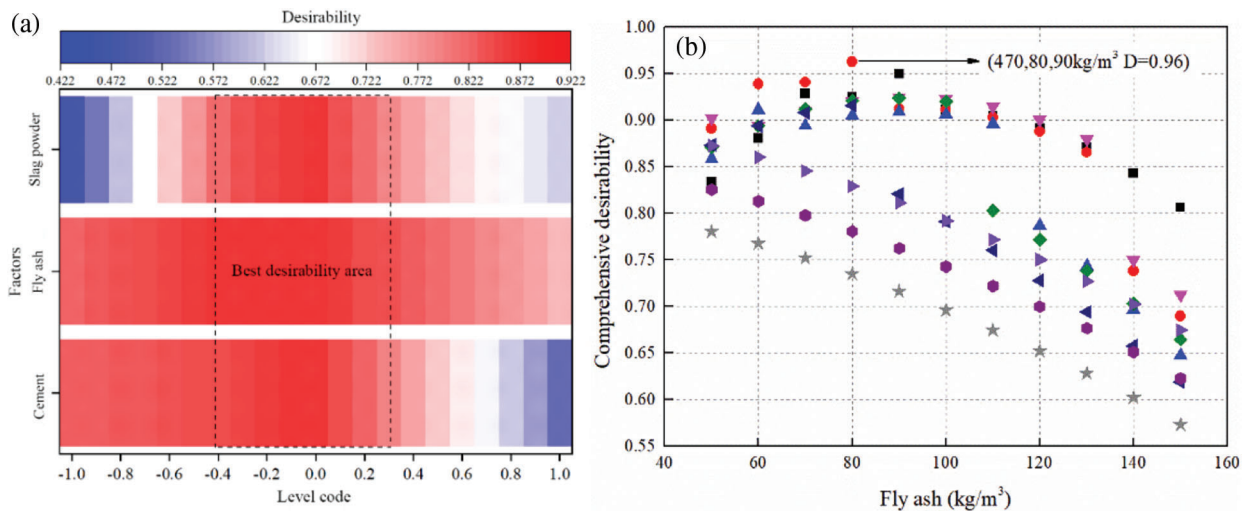


Figure 12: The influence law of different factors on desirability. (a) The influence law of different factors on the desirability; (b) The comprehensive desirability of UCS

3.7.2 The Comparison of Optimization Results

In order to compare with the multi-objective optimization results obtained using RSM-DF, the optimal proportion of the composite cementitious system is found based on RSM, as is shown in Table 6. From Table 6, the optimized mix proportions based on RSM-DF meet the UCS requirements of 7 d, 14 d and 28 d and the UCS at different curing time is not higher than 3% of the UCS index. This indicates that the method adopted in this paper is reliable and can be used for the design and optimize the mix proportion for TWSC. In addition, the UCS of mix proportions obtained by RSM at 7 d and 28 d are lower than the UCS index, which indicates that the method has some disadvantages in terms of multi-objective optimization. The reason for these disadvantages is that TWSC is a complex multiphase composite material with high nonlinearity and uncertainty between factors affecting its strength, so it is difficult to use some specific and reasonable multivariate nonlinear function to predict its mix proportion precisely.

Table 6: Comparison of mix proportions of the composite cementitious system

Methodology	Mix proportion (kg/m ³)			UCS (MPa)					
	Cement	Fly ash	Slag powder	7 d	Index	14 d	Index	28 d	Index
RSM	460	70	90	18.69	18.80	21.37	21.20	22.84	23.50
RSM-DF	470	80	90	19.12		21.75		23.54	

4 Conclusions

In this paper, the effect of the composite cementitious system on the strength of TWSC is studied by RSM and IE is introduced to evaluate the composite cementitious system. In addition, the mix proportion of the composite cementitious system is optimized by RSM-DF.

1. A nonlinear regression model with the content of cement, fly ash and slag powder as variables and the strength of TWSC as the response value is constructed by RSM. The maximum error of the model is only 3.1%, which indicates that the model has a high prediction accuracy. The model can be used to rapidly obtain the strength of the TWSC according to different proportions, which makes the composite cementitious material investigated in this paper have a better practical application value.
2. The strength of TWSC is gradually enhanced with the increase of cement and slag powder content and is first enhanced and then weakened with the increase of fly ash content. When the amount of fly ash content is more than 95 kg/m³, the strength of TWSC is no longer enhanced. Therefore, the dosage of fly ash should be kept below 95 kg/m³ in the investigation of the optimal proportion. In addition, further experiments should be conducted to analyze the role played by fly ash in the composite cementitious material and the reasons for the existence of a critical dosage.
3. The higher the comprehensive score of the composite cementitious system, the better the internal structure of the TWSC. A high comprehensive score means the composite cementitious system is better. The hydration products from the hydration reaction form a dense cement structure, which improves the strength of the TWSC.
4. The optimum mix proportion of the composite cementitious system is obtained based on RSM-DF. The composite cementitious system has a maximum satisfaction of 0.96 when cement, fly ash, and slag powder are mixed at 470, 80 and 90 kg/m³, respectively. It should be noted that this proportion corresponds to TWSC of C20 strength grade, and for underground mines, the deeper mining depth further increases the strength requirement of TWSC, so further experiments should be conducted to

investigate the mechanism of the composite cementitious system and the optimal proportion under the requirement of high strength grade.

Funding Statement: This work is funded by the National Key Research and Development Program of China (Grant Nos. 2018YFC1900603, 2018YFC0604604).

Author Contributions: Yafei Hu: Conceptualization, Methodology, Writing original draft, Writing-review&editing. Keqing Li: Writing-original draft, Writing-review&editing. Lujing Zheng: Methodology, Writing original draft. Bin Han: Conceptualization, Methodology, Writing-original draft, Writing-review&editing.

Conflicts of Interest: The authors declare that they have no conflicts of interest to report regarding the present study.

References

1. Sun, W., Wu, D., Liu, H., Qu, C. (2021). Thermal, mechanical and ultrasonic properties of cemented tailings backfill subjected to microwave radiation. *Construction and Building Materials*, 313, 125535. DOI 10.1016/j.conbuildmat.2021.125535.
2. Qi, C., Chen, Q., Dong, X., Zhang, Q., Yaseen, Z. M. (2020). Pressure drops of fresh cemented paste backfills through coupled test loop experiments and machine learning techniques. *Powder Technology*, 361, 748–758. DOI 10.1016/j.powtec.2019.11.046.
3. Qi, C., Fourie, A., Chen, Q. (2018). Neural network and particle swarm optimization for predicting the unconfined compressive strength of cemented paste backfill. *Construction and Building Materials*, 159, 473–478. DOI 10.1016/j.conbuildmat.2017.11.006.
4. Yin, S., Chen, W., Wang, Y. (2021). Effect of mixed bacteria on cemented tailings backfill: Economic potential to reduce binder consumption. *Journal of Hazardous Materials*, 411, 125114. DOI 10.1016/j.jhazmat.2021.125114.
5. Qi, C., Guo, L., Ly, H., Le, H. V., Pham, B. T. (2021). Improving pressure drops estimation of fresh cemented paste backfill slurry using a hybrid machine learning method. *Minerals Engineering*, 163, 106790. DOI 10.1016/j.mineng.2021.106790.
6. Zhao, X., Zhang, H., Zhu, W. (2014). Fracture evolution around pre-existing cylindrical cavities in brittle rocks under uniaxial compression. *Transactions of Nonferrous Metals Society of China*, 24, 806–815. DOI 10.1016/S1003-6326(14)63129-0.
7. Wang, C., Hou, X., Liao, Z., Chen, Z., Lu, Z. (2019). Experimental investigation of predicting coal failure using acoustic emission energy and load-unload response ratio theory. *Journal of Applied Geophysics*, 161, 76–83. DOI 10.1016/j.jappgeo.2018.12.010.
8. Yu, Z., Shi, X., Chen, X., Zhou, J., Qi, C. et al. (2021). Artificial intelligence model for studying unconfined compressive performance of fiber-reinforced cemented paste backfill. *Transactions of Nonferrous Metals Society of China*, 31, 1087–1102. DOI 10.1016/S1003-6326(21)65563-2.
9. Chen, Q. S., Zhang, Q. L., Wang, X. M., Xiao, C. C., Hu, Q. (2016). A hydraulic gradient model of paste-like crude tailings backfill slurry transported by a pipeline system. *Environmental Earth Sciences*, 75, 1099. DOI 10.1007/s12665-016-5895-8.
10. Chen, Q., Tao, Y., Feng, Y., Zhang, Q., Liu, Y. (2021). Utilization of modified copper slag activated by Na₂SO₄ and CaO for unclassified lead/zinc mine tailings based cemented paste backfill. *Journal of Environmental Management*, 290, 112608. DOI 10.1016/j.jenvman.2021.112608.
11. He, Y., Zhang, Q., Chen, Q., Bian, J., Qi, C. et al. (2021). Mechanical and environmental characteristics of cemented paste backfill containing lithium slag-blended binder. *Construction and Building Materials*, 271, 121567. DOI 10.1016/j.conbuildmat.2020.121567.
12. Qi, C., Chen, Q., Fourie, A., Tang, X., Zhang, Q. et al. (2019). Constitutive modelling of cemented paste backfill: A data-mining approach. *Construction and Building Materials*, 197, 262–270. DOI 10.1016/j.conbuildmat.2018.11.142.

13. Wu, D., Sun, W., Liu, S., Qu, C. (2021). Effect of microwave heating on thermo-mechanical behavior of cemented tailings backfill. *Construction and Building Materials*, 266, 121180. DOI 10.1016/j.conbuildmat.2020.121180.
14. Wu, D., Deng, T., Zhao, R. (2018). A coupled THMC modeling application of cemented coal gangue-fly ash backfill. *Construction and Building Materials*, 158, 326–336. DOI 10.1016/j.conbuildmat.2017.10.009.
15. Chen, X., Shi, X., Zhou, J., Du, X., Chen, Q. et al. (2019). Effect of overflow tailings properties on cemented paste backfill. *Journal of Environmental Management*, 235, 133–144. DOI 10.1016/j.jenvman.2019.01.040.
16. Chen, X., Shi, X., Zhou, J., Yu, Z., Huang, P. (2020). Determination of mechanical, flowability, and microstructural properties of cemented tailings backfill containing rice straw. *Construction and Building Materials*, 246, 118520. DOI 10.1016/j.conbuildmat.2020.118520.
17. Steindl, F. R., Galan, I., Baldermann, A., Sakoparnig, M., Briendl, L. et al. (2020). Sulfate durability and leaching behaviour of dry-and wet-mix shotcrete mixes. *Cement and Concrete Research*, 137, 106180. DOI 10.1016/j.cemconres.2020.106180.
18. Chen, L., Ma, G., Liu, G., Liu, Z. (2019). Effect of pumping and spraying processes on the rheological properties and air content of wet-mix shotcrete with various admixtures. *Construction and Building Materials*, 225, 311–323. DOI 10.1016/j.conbuildmat.2019.07.104.
19. Chen, Q., Tao, Y., Zhang, Q., Qi, C. (2022). The rheological, mechanical and heavy metal leaching properties of cemented paste backfill under the influence of anionic polyacrylamide. *Chemosphere*, 286, 131630. DOI 10.1016/j.chemosphere.2021.131630.
20. Zhang, H., Li, B., Wei, Y., Wang, H. (2021). The settling behavior of matte particles in copper slag and the new technology of copper slag cleaning. *Journal of Materials Research and Technology*, 15, 6216–6230. DOI 10.1016/j.jmrt.2021.11.061.
21. Chen, Q. S., Sun, S. Y., Liu, Y. K., Qi, C. C., Zhou, H. B. et al. (2021). Immobilization and leaching characteristics of fluoride from phosphogypsum-based cemented paste backfill. *International Journal of Minerals Metallurgy and Materials*, 28, 1440–1452. DOI 10.1007/s12613-021-2274-6.
22. Liu, Z., Takasu, K., Koyamada, H., Suyama, H. (2022). A study on engineering properties and environmental impact of sustainable concrete with fly ash or GGBS. *Construction and Building Materials*, 316, 125776. DOI 10.1016/j.conbuildmat.2021.125776.
23. BrabinWinsley, J. B., Muthukannan, M. (2022). A study on strength parameters of concrete with expanded fly ash clay aggregate. *Materials Today: Proceedings*, 56, 3484–3489. DOI 10.1016/j.matpr.2021.11.128.
24. Teng, Y., Liu, S., Zhang, Z., Xue, J., Guan, X. (2022). Effect of triethanolamine on the chloride binding capacity of cement paste with a high volume of fly ash. *Construction and Building Materials*, 315, 125612. DOI 10.1016/j.conbuildmat.2021.125612.
25. Zhang, J., Shi, C., Zhang, Z., Hu, X. (2022). Reaction mechanism of sulfate attack on alkali-activated slag/fly ash cements. *Construction and Building Materials*, 318, 126052. DOI 10.1016/j.conbuildmat.2021.126052.
26. Teixeira, E. R., Camões, A., Branco, F. G. (2022). Synergetic effect of biomass fly ash on improvement of high-volume coal fly ash concrete properties. *Construction and Building Materials*, 314, 125680. DOI 10.1016/j.conbuildmat.2021.125680.
27. Zhao, Y., Gao, J., Xu, Z., Li, S., Luo, X. et al. (2021). Combined effect of slag and clay brick powder on the hydration of blended cement. *Construction and Building Materials*, 299, 123996. DOI 10.1016/j.conbuildmat.2021.123996.
28. Du, C., Tan, H., Jian, S., Wang, J., Shi, T. (2021). Compressive strength and hydration process of sodium carbonate-activated superfine slag/marble powder binders. *Journal of Building Engineering*, 43, 103121. DOI 10.1016/j.job.2021.103121.
29. Zhang, D., Zhao, K., Li, H., Wang, D., Wang, L. et al. (2021). Dispersion properties of fly ash–slag powders under the different environment. *Construction and Building Materials*, 296, 123649. DOI 10.1016/j.conbuildmat.2021.123649.
30. Aydın, S., Baradan, B. (2021). Sulfate resistance of alkali-activated slag and portland cement based reactive powder concrete. *Journal of Building Engineering*, 43, 103205. DOI 10.1016/j.job.2021.103205.

31. Han, Y., Lin, R., Wang, X. (2022). Performance of sustainable concrete made from waste oyster shell powder and blast furnace slag. *Journal of Building Engineering*, 47, 103918. DOI 10.1016/j.jobe.2021.103918.
32. Pandey, A., Gupta, A., Sunny, A., Kumar, S., Srivastava, S. (2020). Multi-objective optimization of media components for improved algae biomass, fatty acid and starch biosynthesis from *Scenedesmus* sp. ASK22 using desirability function approach. *Renewable Energy*, 150, 476–486. DOI 10.1016/j.renene.2019.12.095.
33. Barreno-Avila, E., Moya-Moya, E., Pérez-Salinas, C. (2022). Rice-husk fiber reinforced composite (RFRC) drilling parameters optimization using RSM based desirability function approach. *Materials Today: Proceedings*, 49, 167–174. DOI 10.1016/j.matpr.2021.07.498.
34. Yan, L., Zhang, S., Liu, H., Wang, W., Chen, P. et al. (2016). Optimization of magnetosome production by *acidithiobacillus ferrooxidans* using desirability function approach. *Materials Science and Engineering: C*, 59, 731–739. DOI 10.1016/j.msec.2015.10.060.
35. Islam, M. A., Sakkas, V., Albanis, T. A. (2009). Application of statistical design of experiment with desirability function for the removal of organophosphorus pesticide from aqueous solution by low-cost material. *Journal of Hazardous Materials*, 170, 230–238. DOI 10.1016/j.jhazmat.2009.04.106.
36. Xu, C., Ni, W., Li, K., Zhang, S., Li, Y. et al. (2019). Hydration mechanism and orthogonal optimisation of mix proportion for steel slag–slag-based clinker-free prefabricated concrete. *Construction and Building Materials*, 228, 117036. DOI 10.1016/j.conbuildmat.2019.117036.
37. Xu, C., Ni, W., Li, K., Zhang, S., Xu, D. (2021). Activation mechanisms of three types of industrial by-product gypsums on steel slag–granulated blast furnace slag-based binders. *Construction and Building Materials*, 288, 123111. DOI 10.1016/j.conbuildmat.2021.123111.
38. Zhang, S., Shi, T., Ni, W., Li, K., Gao, W. et al. (2021). The mechanism of hydrating and solidifying green mine fill materials using circulating fluidized bed fly ash-slag-based agent. *Journal of Hazardous Materials*, 415, 125625. DOI 10.1016/j.jhazmat.2021.125625.
39. Zhang, Y., Zhang, S., Ni, W., Yan, Q., Gao, W. et al. (2019). Immobilisation of high-arsenic-containing tailings by using metallurgical slag-cementing materials. *Chemosphere*, 223, 117–123. DOI 10.1016/j.chemosphere.2019.02.030.
40. Adamu, M., Trabanpruek, P., Jongvivatsakul, P., Likitlersuang, S., Iwanami, M. (2021). Mechanical performance and optimization of high-volume fly ash concrete containing plastic wastes and graphene nanoplatelets using response surface methodology. *Construction and Building Materials*, 308, 125085. DOI 10.1016/j.conbuildmat.2021.125085.
41. Zhu, L., Jin, Z., Zhao, Y., Duan, Y. (2021). Rheological properties of cemented coal gangue backfill based on response surface methodology. *Construction and Building Materials*, 306, 124836. DOI 10.1016/j.conbuildmat.2021.124836.
42. Xie, S., Kumagai, S., Kameda, T., Saito, Y., Yoshioka, T. (2021). Prediction of pyrolyzate yields by response surface methodology: A case study of cellulose and polyethylene co-pyrolysis. *Bioresource Technology*, 337, 125435. DOI 10.1016/j.biortech.2021.125435.
43. Savari, C., Sotudeh-Gharebagh, R., Kulah, G., Koksai, M., Mostoufi, N. (2019). Detecting stability of conical spouted beds based on information entropy theory. *Powder Technology*, 343, 185–193. DOI 10.1016/j.powtec.2018.11.028.
44. Wang, W. C., Liu, H. L., Li, F. S., Wang, H., Ma, X. et al. (2021). Effects of unsaturated fatty acid methyl esters on the oxidation stability of biodiesel determined by gas chromatography-mass spectrometry and information entropy methods. *Renewable Energy*, 175, 880–886. DOI 10.1016/j.renene.2021.04.132.
45. Chen, N., Liu, Y., Chen, H., Cheng, J. (2017). Detecting communities in social networks using label propagation with information entropy. *Physica A: Statistical Mechanics and its Applications*, 471, 788–798. DOI 10.1016/j.physa.2016.12.047.
46. Takino, K., Ishinagi, Y. (2022). On mean–variance analysis of a bank’s behavior. *Finance Research Letters*, 46, 102292. DOI 10.1016/j.fl.2021.102292.

47. Moein Darbari, A., Alavi, M. A., Saleh, S. R., Nejati, V. (2022). Sensitivity analysis of nanofluid flow over different flat tubes confined between two parallel plates using taguchi method and statistical analysis of variance. *International Journal of Thermal Sciences*, 173, 107428. DOI 10.1016/j.ijthermalsci.2021.107428.
48. Bayisa, Y. M., Bullo, T. A. (2021). Optimization and characterization of oil extracted from croton macrostachyus seed for antimicrobial activity using experimental analysis of variance. *Heliyon*, 7, e08095. DOI 10.1016/j.heliyon.2021.e08095.
49. Liu, G., Li, L., Yang, X., Guo, L. (2016). Stability analyses of vertically exposed cemented backfill: A revisit to mitchell's physical model tests. *International Journal of Mining Science and Technology*, 26, 1135–1144. DOI 10.1016/j.ijmst.2016.09.024.
50. Ju, F., Huang, P., Guo, S., Xiao, M., Lan, L. (2017). A roof model and its application in solid backfilling mining. *International Journal of Mining Science and Technology*, 27, 139–143. DOI 10.1016/j.ijmst.2016.11.001.
51. Zhao, L. (2021). Numerical investigation on the mechanical behaviour of combined backfill-rock structure with KCC model. *Construction and Building Materials*, 283, 122782. DOI 10.1016/j.conbuildmat.2021.122782.